TROPICAL AGRONOMIC RESEARCH AND HIGHER EDUCATION CENTER

EDUCATION DIVISION

POSTGRADUATE PROGRAM

Estimation of aquifer recharge measured by the isotopic fractionation of water vapor and the hydrological balance of the soil in the dry tropical forest of Costa Rica

A thesis submitted for consideration by the Education Division and the Postgraduate Program as a requirement to qualify for the degree of

MAGISTER SCIENTIAE

in Integrated Watershed Management

Andrea Noemí Barrientos Peña
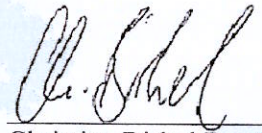
Turrialba, Costa Rica

2022

This Master's thesis has been accepted in its present form by the Division of Education and the Graduate School Program of CATIE and by the advisory committee of the student, considering that it fills the requirements necessary for the student to present the final defense as well as participate in the final exam

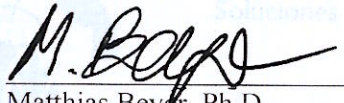### *MAGISTER SCIENTIAE* IN INTEGRATED WATERSHED MANAGEMENT
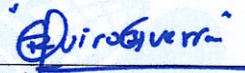
SIGNATORIES:

_____
Laura Benegas Negri, Ph.D.
Thesis co-director

_____
Christian Birkel Dostal, Ph.D.
Thesis co-director

_____
Matthias Beyer, Ph.D.
Member of the Advisory Committee

_____
Roberto Quiroz Guerra, Ph.D.
Dean of the Graduate School

_____
Andrea Noemí Barrientos Peña
Candidate

DEDICATION

For those who are new to this exciting path of hydrology and modeling. To those who believe that through science, we can transform realities, affect our environment, and have a positive impact on society to achieve sustainable development.

To my fellow women scientists, brave women who are building a path even with differentiated conditions and risks.

To God Romans 11:36.

ACKNOWLEDGMENTS

First, to God for paving the way to get here. Romans 11:36.

To my family for their unconditional supportand words of encouragement, for motivating me to be better, and teaching me by example. For reminding me with their wise words: "This is not a sprint race, but an endurance race."

To my fiancé for always being there for me and cheering me on.

To the friends I already had and the ones I made along this path. To my friends from CATIE who made this experience more fun and fuller of memories.

To my advisors who have taught me a lot with patience, and for sharing their passion for science.

To the German Academic Exchange Service, for supporting Central American students and strengthening the human talent of our countries.

CONTENT INDEX

FIGURES INDEX

TABLES INDEX

LIST OF ACRONYMS

^{2}H: Deuterium
AET: Actual evapotranspiration in mm
alpha: Interception threshold parameter
AT: Air temperature
C-G: Craig and Gordon
CRDS: Cavity ring-down spectroscopy
Datm: Deuterium in atmospheric water vapor
EEFH: Estación Experimental Forestal Horizontes
Ei: Interception evaporation in mm
Es: Soil evaporation in mm
ET: Evapotranspiration in mm
fupCSTO_D: Deuterium concentration in upper storage (fractionation involved)
g1: Nonlinear scaling parameter of upper horizon, if g1=1 linear case.
g2: Nonlinear scaling parameter of lower horizon, if g2=1 linear case.
g3: Nonlinear scaling parameter of deep horizon, if g3=1 linear case.
GMWL: Global Meteoric Water Line
GW_D: Deuterium in groundwater
GW: Lower soil horizon storage in mm
gwCQ_D: Simulated deuterium discharge concentration in lower storage
gwCSTO_D: Deuterium concentration in lower storage
GWflow: Groundwater flow from lower soil horizon in mm
GWmax: Maximum measured soil moisture content lower horizon
gwSp: Passive lower storage mixing volume
Ic: Maximum infiltration capacity
INTp: Passive interception storage mixing volume
k: Seasonality factor
KGE: Kling-Gupta efficiency
ks1: Saturated hydraulic conductivity upper soil horizon
ks2: Saturated hydraulic conductivity lower soil horizon
ks3: Saturated hydraulic conductivity deepest horizon
LAI: Leaf area index
LEL: Local Evaporative Line

Lmax: Maximum measured soil moisture content deeper horizon
lowCQ_D: Simulated deuterium discharge concentration in deep storage
lowCSTO_D: Deuterium concentration in deep storage
lowSp: Passive deep storage mixing volume
OF: Objective function
P_D: Deuterium in precipitation
P: Precipitation
Perc: Percolation in mm
PET: Potential evapotranspiration
PF_Scale: Preferential flowpath parameter
rE: Extinction factor
RH: Relative humidity
Sdeep: Deep soil horizon storage in mm
Smax: Maximum measured soil moisture content upper horizon
SR: Solar radiation
STO: Upper soil horizon storage in mm
stoSp: Passive upper storage mixing volume
SW2_150_D: Deuterium in soil water 150 cm depth
SW2_150cm: Soil water content 70 - 150 cm depth
SW2_20_D: Deuterium in soil water 20 cm depth
SW2_30cm: Soil water content 30 cm depth
SW2_50_D: Deuterium in soil water 50 cm depth
SW2_70cm: Soil water content 30 - 70 cm depth
Tobs: Observed transpiration
Tr: Transpiration in mm
upCQ_D: Simulated deuterium discharge concentration in upper storage
upCSTO_D: Deuterium concentration in upper storage
VSMOW: Vienna Standard Mean Ocean Water
WV_D: Isotopic content of water vapor
x: Water vapor mixing ratio

Estimation of aquifer recharge measured by the isotopic fractionation of water vapor and the hydrological balance of the soil in the dry tropical forest of Costa Rica

Andrea N. Barrientos[1]
Christian Birkel[2]
Laura Benegas[1]
Matthias Beyer[3]

Abstract

The dry tropical forest is one of the most vulnerable in Costa Rica and one of the rarest in Central America. It is in the north pacific of Costa Rica, which presents markedly seasonal rains with several months of drought. These droughts cause severe environmental disturbances in the dry tropical forests (Leiva et al. 2009). This northern region presents the most days without rain in the country, which is why it is considered highly vulnerable due to its low hydric availability (Echeverría Bonilla 2011). In this context of water scarcity, inappropriate and irrational exploitation of groundwater is generated (GWP 2016). Better hydrological monitoring efforts are required to obtain effective water resource management that considers the resilience of groundwater in the context of climate change, especially in the Dry Corridor of Central America (Sánchez-Murillo and Birkel 2016).
We developed the first approach of an hourly, lumped, conceptual, tracer-aided water balance model that simulates aquifer recharge in a dry tropical forest in Costa Rica. The model considers evaporative fractionation by estimating the isotopic content of the vapor losses from interception and the upper soil horizon, which is a process commonly overlooked. The incorporation of fractionation in the model resulted in satisfactory representations of the behavior and variability of the isotopic signals in atmospheric water vapor. A first effort was made to estimate the recharge based on the model with the best metrics. Simulations show that a recharge of 89 mm was generated from March to December 2019.

Keywords: hydrology, isotopes, recharge, fractionation

[1] Tropical Agricultura Research and Higher Education Center, CATIE, Turrialba, Costa Rica
[2] Department of Geography and Water and Global Change Observatory, University of Costa Rica, San Jose, Costa Rica
[3] Institute for Geoecology, Technische Universität Braunschweig, Braunschweig, Germany

1. Introduction

The dry tropical forest is one of the most vulnerable in Costa Rica and one of the rarest in Central America. It is in the north pacific of Costa Rica, which presents markedly seasonal rains with several months of drought. These droughts cause severe environmental disturbances in the dry tropical forests (Leiva et al. 2009). This northern region presents the most days without rain in the country, which is why it is considered highly vulnerable due to its low hydric availability (Echeverría Bonilla 2011). In this context of water scarcity, inappropriate and irrational exploitation of groundwater is generated (GWP 2016). Various studies by Servicio de Aguas Subterráneas, Riego y Avenamiento, show several aquifers in the north pacific (Potrero, Brasilito, Nimboyores, and Huacas-Tamarindo) have limited availability of the resource for its use caused by a high degree of exploitation and intervention (SENARA 2016).

The aquifers have enormous social, human, cultural, and socioeconomic value because they store freshwater for consumption supply and are a fundamental element for the integrated management of water resources (SENARA 2020). Therefore, it is necessary to monitor the water resource to achieve integrated management. Monitoring the response of an aquifer and its behavior is essential to achieve effective groundwater management and to control the impacts of its extraction.

Considering the above, better hydrological monitoring efforts are required to obtain effective water resource management and management plans that consider the resilience of groundwater in the context of climate change, especially in the Dry Corridor of Central America (Sánchez-Murillo and Birkel 2016). This can be achieved through hydrological cycle studies. The hydrological cycle repeatedly studies the water from its evaporation, precipitation, infiltration, runoff, and evapotranspiration until its return to the atmosphere and the ocean. In other words, the hydrological cycle studies the movement of water from its formation to precipitation until it falls to the ground (Brauman 2015).

One field of hydrology that studies the hydrological cycle is isotope hydrology, which uses stable or radioactive isotopes artificially or naturally found in the environment. This technique uses environmental isotopes such as hydrogen and oxygen in water molecules (IMTA 2009). Identifying these isotopes allows for characterizing the dynamic behavior of water in the hydrological cycle (Archana et al. 2014). For example, when water evaporates or condenses, it is marked by an isotopic footprint that varies according to its path in the cycle. This footprint allows elucidating from its evaporation, precipitation, infiltration, runoff, and evapotranspiration, until its return to the atmosphere and the ocean, and repeatedly.

Given the above, isotope techniques allow an understanding of the water cycle's components, helping to assess better the quantity, quality, and sustainability of water (Ortega and Gil 2019). They help to provide rapid hydrological information for large areas. These techniques are crucial in global efforts to assess and manage water resources (IAEA 2004). Additionally, in the hydrological cycle, groundwater is the least understood component. To better understand groundwater, natural isotopes are used as tracers to determine where it is recharged, where it comes from, what the underground movement is like, and if it is vulnerable to contamination or changes in climatic conditions.

Despite isotope hydrology allows the study of hydrological and groundwater processes at low costs compared to continuous monitoring that is usually not feasible in developing countries (Iraheta 2019), even today, the variations in stable isotopes and groundwater recharge mechanisms are poorly understood in the tropic of Central America (Sánchez-Murillo and Birkel 2016). Collecting isotopic data from a decade provides essential insights into the dynamics of the hydrological cycle (Sánchez-Murillo et al. 2013).

Although the evaporation of water from the oceans and the terrestrial environment governs the global water cycle and climate (Gonfiantini et al. 2018), there is still uncertainty in this component of the hydrological cycle. Evapotranspiration is an important source of uncertainty in inland water flows and land surface modeling (Schlaepfer et al. 2014). Stable isotopes help to reduce this uncertainty since they are excellent tracers for monitoring and quantifying the evaporation at global and regional scales because the stable hydrogen and oxygen isotope ratios in the water molecule are isotopically partitioned during evaporation since the heavier isotopes tend to be retained in residual water. This process gave origin to the well-known Craig-Gordon model (C-G).

Given this uncertainty, the Craig-Gordon model aids in obtaining better estimates of the fractionation of hydrogen and oxygen isotopes during water evaporation under natural conditions and can be used to optimize models of hydrological balance.

Taking the above into consideration, this thesis sought to implement isotope hydrology to fit an isotope-adjusted soil hydrological model using the Craig-Gordon model to estimate the isotopic fractionation that contributes to a more precise estimate of aquifer recharge in a plot in the dry tropical forest in Costa Rica in 2019, using atmospheric water vapor and soil water isotope data and soil moisture measurements.

The specific objectives were to:
1. Compare the isotopic composition of atmospheric water vapor obtained from 1) the Craig-Gordon model and 2) in situ measured atmospheric water vapor recorded from March to May 2019 in a dry tropical forest.
2. Conceptualize an hourly hydrological model of the soil (at soil profile scale) coupled with isotopic data of atmospheric water vapor and soil water and soil moisture measurements.
3. Estimate the aquifer recharge of the study plot in a tropical dry forest in Costa Rica for the year 2019 using the calibrated model.

2. Study site

The Estación Experimental Forestal Horizontes (EEFH) is in the northwest of Costa Rica, located within the Área de Conservación Guanacaste. The long-term average annual rainfall is 1 575 mm. Despite the above, the area has an accumulated precipitation per year from 880 to 3 030 mm, showing significant variability throughout the year caused by El Niño-Southern Oscillation (Powers et al. 2009; Waring et al. 2019). Precipitation is very seasonal, occurring mainly between May and November (Waring et al. 2019). The total precipitation of the 2018 rainy season was 1 571 mm, similar to the long-term annual average (Instituto Meteorológico Nacional 2020). In 2018, the average temperature was $27 \pm 4\,°$ C, above the long-term average (Kühnhammer et al. 2022).

The soils at the Estación Experimental Forestal Horizontes are of volcanic origin and have a high clay content, about 38% (Alfaro et al. 2001; Waring et al. 2019). The soil is classified as Vertisol at the specific data collection site and has a clay loam texture. The average values for sand content are $26 \pm 10\%$, silt $36 \pm 5\%$, and clay $37 \pm 9\%$ (Kühnhammer et al. 2022).

The area where the EEFH is located now, was used for decades for rice production and cattle grazing, among other agricultural uses. However, currently, it is a regenerating tropical dry forest (Werden et al. 2018).

Figure 1. Location of Estación Experimental Forestal Horizontes in the northwest of Costa Rica.

3. Methodology

3.1. Hydrometeorological and Isotope Data

The isotope data was collected in 2019 from March to May, from the dry season to the beginning of the transition season. Specifically, isotopic precipitation data were collected from the Libera station (located 30 km from EEFH). Meanwhile, the hydrometeorological data were collected from March to December of the same year. An automated weather station (HOBO RX3000 weather station, Onset Computer Corporation) recorded precipitation, solar radiation, air temperature, and relative humidity since February 2019. Isotope values ($\delta2H$ and $\delta18O$) were measured with a cavity ring-down spectroscopy (CRDS) analyzer (L2130-i, Picarro Inc.) and reported in the delta-notion of the relative deviation from the Vienna Standard Mean Ocean Water (VSMOW) standard (Kühnhammer et al. 2022). In addition, soil water at different depths was recorded with capacitance moisture sensors (Odyssey® Xtreem Multi-Profile Soil Moisture Logger and Sensor).

The isotope and soil water content data used for the elaboration of the model, was explicitly taken from the observation plot of the native tree species *Sideroxylon capiri*, commonly known as "Tempisque"; during the dry season, this tree species don't shed its foliage, which means it continues to transpire and absorb water from the soil (Kühnhammer et al. 2022). Observed transpiration values were determined by upscaling sap flux measurements, and potential evapotranspiration was calculated through Penman-Monteith.
Summaries of all measurements used as input data are in Table 1.

Table 1. Summary statistics of hydrometeorological characteristics and isotope values (with unit, n number of samples, mean, range, and coefficient of variation CV) incorporated into the model from March 14th to December 29th 2019.

Data	Unit	n	Mean	Range [min, max]	CV
Hydrometeorology					
Precipitation (P)	mm	6964	0.12	[0, 98.6]	12.3
Solar radiation (SR)	W/m^2	6964	129.7	[1, 1187.5]	1.8
Air temperature (AT)	ºC	6964	26.7	[18.7, 42]	0.16
Relative humidity (RH)	%	6964	82.4	[21.4, 100]	0.23
Leaf area index (LAI)		6964	2.9	[1, 3.6]	0.31
Potential evapotranspiration (PET)	mm	6964	0.21	[0, 1.8]	1.7
Transpiration (Tobs)	mm	2710	0.11	[0, 0.6]	0.92
Soil water content 30 cm depth (SW2_30cm)	mm	6737	57.6	[8.5, 140.5]	0.4
Soil water content 30 - 70 cm depth (SW2_70cm)	mm	6635	99.8	[31.7, 181.8]	0.33
Soil water content 70 - 150 cm depth (SW2_150cm)	mm	4108	148.4	[40.6, 398]	0.39
Isotopic (δ^2H)					
Soil water 20 cm depth (SW2_20_D)	‰	23	-42.3	[-66, -10.5]	0.41
Soil water 50 cm depth (SW2_50_D)	‰	23	-68.8	[-85.2, -54.45]	0.14
Soil water 150 cm depth (SW2_150_D)	‰	23	-65.9	[-82, -50]	0.14
Precipitation (P_D)	‰	419	-45.7	[-111.7, 10.7]	0.5
Groundwater (GW_D)	‰	2	-51.6	[-52.1, -51.1]	0.01
Atmospheric water vapor (Datm)	‰	89	-98	[-153.23, -66]	0.29

3.2. Tracer-Based Modeling Approach

3.2.1. The Model
The model philosophy consists of a conceptual hydrological model with tracer coupling. The tracer data were incorporated into the model with continuous water and tracer simulation through water and mass balance equations. The model is a lumped, conceptual, tracer-aided water balance model that simulates aquifer recharge (Figure 2). The input data were hydrometeorological records and isotope data, summarized in Table 1.

The structure of the model is composed of three reservoirs: 0 - 30 cm, 30 - 70 cm, and 70 - 150 cm. This is because dissimilar isotopic behavior was observed in the different soil horizons (Table 1, Figure 3). The loss in the third reservoir is the estimation of the aquifer recharge. The recharge is the flow simulated as a loss of the hydrological balance since it is a one-dimensional model. No roots were observed in the field at depths greater than 150 cm, so it is assumed that there will be no influence of capillary flows, evaporation, and transpiration below this depth. Additionally, a routine of interception was considered, and subsequently, partitioned water into evaporation fluxes (soil and interception evaporation), and transpiration from the upper two soil reservoirs was executed.
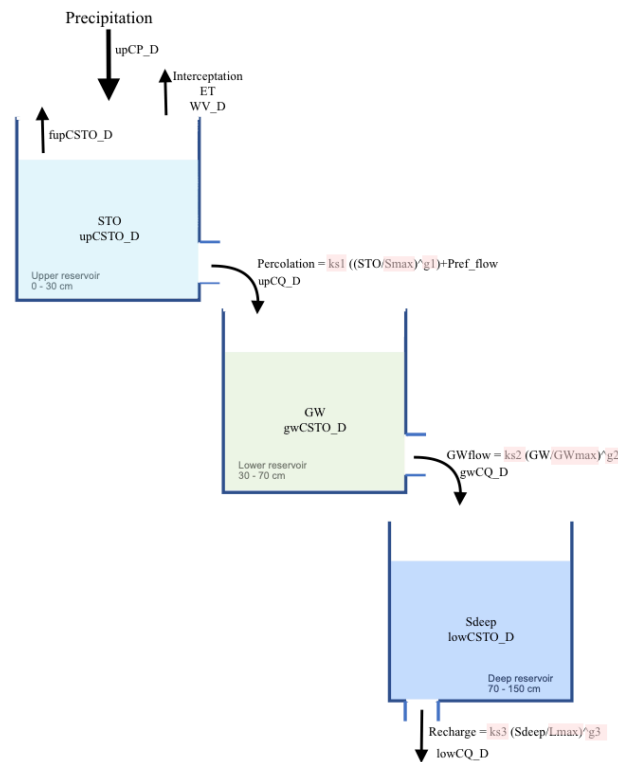
Figure 2. Representative scheme of the model structure with internal state variables (*STO, GW,*and *Sdeep* storage components), and the associated fluxes (*Percolation, GWflow,* and *Recharge*). Evaporation fluxes (*ET*) are indicated, and the concentrations are associated with them (*WV_D* and *fupCSTO_D*). Variables highlighted in red correspond to model parameters. Concentrations (*upCSTO_D, gwCSTO_D,* and *lowCSTO_D*) and fluxes (*upCQ_D, gwCQ_D*, and *lowCQ_D*) for isotopic transport are also shown in the diagram.

The hourly flow-tracer soil model incorporates nineteen parameters: thirteen are employed to simulate fluxes and reservoirs, four mixing volumes, and two are applied for the Craig-Gordon model (Table 2). The model was employed from March to December

2019 and calibrated throughout this period. The involvement of isotopic data to evaluate the state variables and fluxes is presented in Figure 2.

Due to the differences in isotopic composition between the first and deeper reservoirs (Table 1), the interception process was included (Equations 1-3). The initial storage values in each reservoir and isotopic composition were defined according to the observed average of the first month (Equations 4, 6, and 8 for storage and Equations 21, 26, and 28 for isotopic composition). Percolation from the first to the second reservoir is calculated with a non-linear discharge algorithm with a power function (Equation 5). Similarly, Groundwater flow and recharge are calculated (Equations 7 and 9). Regarding the transport of isotopes, each reservoir enables complete mixing with an additional mixture volume (Equations 20, 25, and 27). The potential fractionation due to evaporation at the interception and the first reservoir was included in the model (Equations 19 and 23) due to the isotopic behavior shown in Figure 4. Based on the Craig-Gordon model, the isotopic composition of the residual liquid and the vapor losses were calculated (Equations 16, 17, 22, and 24). Algorithms of model components are shown in Table 3. Calculations and analyzes were performed in the R language.

Table 2. Parameters incorporated to the flow-tracer model.

Parameters	
Hydrometeorology	
rE	Extinction factor
alpha	Interception threshold parameter
Smax	Maximum measured soil moisture content upper horizon
Ic	Maximum infiltration capacity
ks1	Saturated hydraulic conductivity upper soil horizon
ks2	Saturated hydraulic conductivity lower soil horizon
ks3	Saturated hydraulic conductivity deepest horizon
GWmax	Maximum measured soil moisture content lower horizon
Lmax	Maximum measured soil moisture content deeper horizon
g1	Nonlinear scaling parameter of upper horizon, if g1=1 linear case.
g2	Nonlinear scaling parameter of lower horizon, if g2=1 linear case.
g3	Nonlinear scaling parameter of deep horizon, if g3=1 linear case.
PF_Scale	Preferential flow path parameter
Isotopes	
INTp	Passive interception storage mixing volume
stoSp	Passive upper storage mixing volume
gwSp	Passive lower storage mixing volume
lowSp	Passive deep storage mixing volume
Craig-Gordon Model	
k	Seasonality factor
x	Water vapor mixing ratio

Table 3. Model components algorithms.

Model Components	Conceptual Model	Equation	References
Surface cover fraction	$SCF = 1 - e^{rE*LAI}$	1	
Interception threshold	$D = (alpha \cdot LAI) \cdot \left(1 - \left(\dfrac{1}{1 + \dfrac{SCF \cdot P}{alpha \cdot LAI}}\right)\right)$	2	*(Sutanto et al. 2012)*
Net Precipitation	$PN = P - D$	3	*(Sutanto et al. 2012)*
Upper soil horizon storage	$STO = STO + PN$	4	
Percolation	$Perc = ks1 \cdot \left(\dfrac{STO}{Smax}\right)^{g1}$	5	
Lower soil horizon storage	$GW = GW + Perc$	6	
Groundwater flow	$GWflow = ks2 \cdot \left(\dfrac{GW}{GWmax}\right)^{g2}$	7	
Deep soil horizon storage	$Sdeep = Sdeep + GWflow$	8	
Recharge	$Recharge = ks3 \cdot \left(\dfrac{Sdeep}{Lmax}\right)^{g3}$	9	
Equilibrium fractionation factor	$\alpha_e = exp\left[\dfrac{1}{1000} \cdot 1158.8\left(\dfrac{T_k^3}{10^9}\right) - 1620.1\left(\dfrac{T_k^2}{10^6}\right) + 794.84\left(\dfrac{T_k}{10^6}\right) - 2.9992\left(\dfrac{10^9}{T_K^3}\right)\right]$	10	*(Horita y Wesolowski 1994)*
Enrichment factor	$\varepsilon^+ = (\alpha_e - 1) \cdot 1000$	11	
Kinetic fractionation factor	$\varepsilon_k = 0.9755(1 - 0.9755) \cdot 1000 \cdot (1 - RH)$	12	*(Merlivat 1978)*
Atmospheric composition	$\delta_A = \dfrac{\delta_P - k \cdot \varepsilon^+}{1 + k \cdot \varepsilon^+ \cdot 10^{-3}}$	13	*(Gibson et al. 2008)*
Enrichment slope	$m = \dfrac{RH - 10^{-3}(\varepsilon_k + \dfrac{\varepsilon^+}{\alpha_e})}{1 - RH + 10^{-3} + \varepsilon_k}$	14	*(Gibson et al. 2016)*
Limiting isotopic composition	$\delta_* = \dfrac{RH \cdot \delta_A + \varepsilon_k + \varepsilon^+/\alpha_e}{RH - 10^{-3} \cdot (\varepsilon_k + \varepsilon^+/\alpha_e)}$	15	*(Gibson et al. 2016)*
Isotopic content of the residual liquid in interception	$\delta_L = (Int\_CD - \delta_*) \cdot (1 - x)^m + \delta_*$	16	*(Gonfiantini 1986)*
Isotopic content of the evaporating flux in interception	$\delta_{E_I} = \dfrac{\dfrac{(\delta_L - \varepsilon^+)}{\alpha_e} - RH \cdot \delta_A - \varepsilon_k}{(1 - RH + 10^{-3} \cdot \varepsilon_k)}$	17	*(Gibson et al. 2016)*
δ^2H concentration in interception	$Int\_CD = \dfrac{(Int\_D \cdot Int\_CD) + (D \cdot upCP\_D)}{Int\_D + D}$	18	
Isotopic fractionation in interception	$fInt\_CD = \dfrac{(Int\_D \cdot Int\_CD) - (E_i \cdot \delta_L)}{Int\_D - E_i - Th}$	19	

Available mixing volume in upper storage	$upSTO\_D = STO - PN + Es + Tr\_upper + Perc + stoSp$	20	
δ^2H concentration in upper storage	$upCSTO\_D = \dfrac{(upSTO\_D \cdot upCSTO\_D) + (PN \cdot upCP\_D)}{upSTO\_D + PN}$	21	
Isotopic content of the residual liquid in upper storage	$\delta_{L_u} = (upCSTO\_D - \delta_*) \cdot (1 - x)^m + \delta_*$	22	*(Gonfiantini 1986)*
Isotopic fractionation in upper storage	$fupCSTO\_D = \dfrac{(upCSTO\_D \cdot upCSTO\_D) - (E_s \cdot \delta_{L_u})}{UPSTO\_D - E_s - Tr_{upper} - Perc}$ $upCQ\_D = fupCSTO\_D$	23	
Isotopic content of the evaporating flux in upper storage	$\delta_{E_u} = \dfrac{\dfrac{(\delta_{L_u} - \varepsilon^+)}{\alpha_e} - RH \cdot \delta_A - \varepsilon_k}{(1 - RH + 10^{-3} \cdot \varepsilon_k)}$	24	*(Gibson et al. 2016)*
Available mixing volume in lower storage	$gwSTO\_D = GW - Perc - Pref\_Flow + GWflow + Tr\_lower + gwSp$	25	
δ^2H concentration in lower storage	$gwCSTO\_D = \dfrac{(gwSTO\_D \cdot gwCSTO\_D) + (Perc \cdot upCQ\_D)}{gwSTO_D + Perc - GWflow - Tr\_lower}$ $gwCQ\_D = gwCSTO\_D$	26	
Available mixing volume in deep storage	$lowSTO\_D = GWflow + Recharge + Tr\_Deep + lowSp$	27	
δ^2H concentration in deep storage	$lowCSTO\_D = \dfrac{(lowSTO\_D \cdot lowCSTO\_D) + (GWflow \cdot gwCQ\_D)}{lowSTO\_D + GWflow - Recharge - Tr\_deep}$	28	
δ^2H concentration in atmospheric water vapor	$WV\_D = \dfrac{(\delta_{E_I} \cdot E_i) + (\delta_{E_u} \cdot E_s) + (Tr * fupCSTO\_D)}{E_i + E_s + Tr}$	29	

2.4.2. Model Calibration

The model calibration incorporates storage dynamics and isotope dynamics. The impact of distinct data and objective functions (OF) for model calibration in flux and state simulations was evaluated. For both flux and state, the Kling-Gupta efficiency (KGE) goodness-of-fit metric was employed to simplify the analysis of correlation, bias, and variability between observations and simulations (Gupta et al. 2009) (Table 4).

Table 4. Kling-Gupta efficiency metrics for observed data and simulations.

Metric	Observed data	Simulations
Hydrodynamic		
KGE1	SW2_30cm	STO
KGE2	SW2_70cm	GW
KGE3	SW2_150cm	Sdeep
KGE4	Tobs	Tr
Isotopic		
KGE5	SW2_20_D	fupCSTO_D
KGE6	SW2_50_D	gwCSTO_D
KGE7	SW2_150_D	lowCSTO_D
KGE8	Datm	WV_D

The following model modules were addressed for calibration (Table 5):

1) Hydrodynamic module: evaluation of (a) soil water in the upper, lower, and deep storage (*STO, GW, Sdeep*); (b) transpiration (*Tr*); and (c) combination of 1(a) and 1(b).
2) Isotope module: evaluation of (a) isotopic storage concentrations in the different reservoirs (*fupCSTO_D, gwCSTO_D,* and *lowCSTO_D*); (b) isotopic composition of atmospheric water vapor (*WV_D*); (c) combination of 2(a) and 2(b); and (d) isotopic concentrations (*gwCSTO_D* and *WV_D*).
3) Combined module: evaluation of (a) soil water storage 1(a) and isotope data (*gwCSTO_D and WV_D*); and (b) soil water storage (*fupCSTO_D* and *gwCSTO_D*) and isotope data (*gwCSTO_D* and *WV_D*).

Table 5. Objective functions for each calibration module (n number of combined OF).

Calibration Module	Objective Function
Hydrodynamic	
1(a) (n=3)	KGE1, KGE2 & KGE3 > 0.4
1(b) (n=1)	KGE4 > 0
1(c) (n=4)	KGE1, KGE2 & KGE3 > 0.4 & KGE4 > 0
Isotopic	
2(a) (n=3)	KGE5, KGE6 & KGE7 > 0
2(b) (n=1)	KGE8 > 0.1
2(c) (n=4)	KGE5, KGE6 & KGE7 > 0 & KGE8 > 0.1
2(d) (n=2)	KGE6 > 0.6 & KGE8 > 0.05
Combined	
3(a) (n=5)	KGE1, KGE2 & KGE3 > 0.4 & KGE6 > 0 &KGE8 > 0
3(b) (n=4)	KGE1 > 0.2 & KGE2 > 0.2 KGE6 > 0.6 &KGE8 > 0.05

To perform the calibration, the Latin Hypercube (LH) random sampling was used for parameter values definition, because it supplies a complete hedge of each parameter range from their distributions (Farzamian et al. 2017). The LH significantly decreases large numbers of iterations to achieve a reasonable result (Birkel et al. 2014). Since a "global minimum for a model with large number of parameters will be difficult to achieve" (Beven 2006 cited by Birkel et al. 2014), referring to the complexity of constraining the parameter spectrum, a wide range of each parameter is initially set (Table 6). The stratified Monte Carlo sampling, Latin Hypercube, with 10 000 iterations was implemented to explore these ranges. The best set of parameters was used to generate storage and flow simulations according to each objective function (hydrodynamic, isotope, or combined).

Table 6. Initial model parameter range, mean values, and 5th and 95th percentile (after applying Latin Hypercube random sampling).

Parameter values	rE	alpha	Smax (mm)	Ic (mm/h)	ks1	ks2	ks3	GWmax (mm)	Lmax (mm)	g1	g2	g3	PF_Scale	INTp (mm)	stoSp (mm)	gwSp (mm)	lowSp (mm)	k	x
Initial range [min, max]	[-0.4, -0.1]	[1, 5]	[400, 700]	[57.6, 57.6]	[2.1, 15]	[5, 20]	[5, 20]	[274, 450]	[200, 500]	[2, 3.75]	[3, 5]	[3, 5]	[0.1, 0.8]	[1, 100]	[200, 1000]	[2, 100]	[1, 100]	[0.25, 0.9]	[0.25, 0.75]
Mean	-0.25	3	550	57.6	8.55	12.5	12.5	362	350	2.87	4	4	0.45	50.5	600	51	50.5	0.57	0.5
5th and 95th percentiles	[-0.32, -0.17]	[2, 4]	[475, 625]	[57.6, 57.6]	[5.32, 11.76]	[8.75, 16.25]	[8.75, 16.25]	[318, 406]	[275, 425]	[2.43, 3.31]	[3.5, 4.5]	[3.5, 4.5]	[0.27, 0.62]	[25.75, 75.25]	[400, 800]	[26.5, 75.49]	[25.75, 75.24]	[0.41, 0.74]	[0.37, 0.62]

Note: for parameter meanings see Table 2.

4. Results

4.1. Hydrometeorological and Tracer Dynamic

A total of 873.2 mm of precipitation was recorded in the study period, which was close to the previously reported accumulated precipitation values (Powers et al. 2009; Waring et al. 2019). Although the measurements from January to mid-March are missing, it can be observed that it was a drier year since the accumulated value of precipitation is closer to the lower range. The behavior of the precipitation was very seasonal; however, that year occurred mainly from April to October in contrast to what was expected (May to November). Three major precipitation events were recorded in October with 98.6, 26, and 31 mm values. In these events, runoff generation was observed in the field. March and April 2019 showed the warmest months of the study period with increased evapotranspiration.
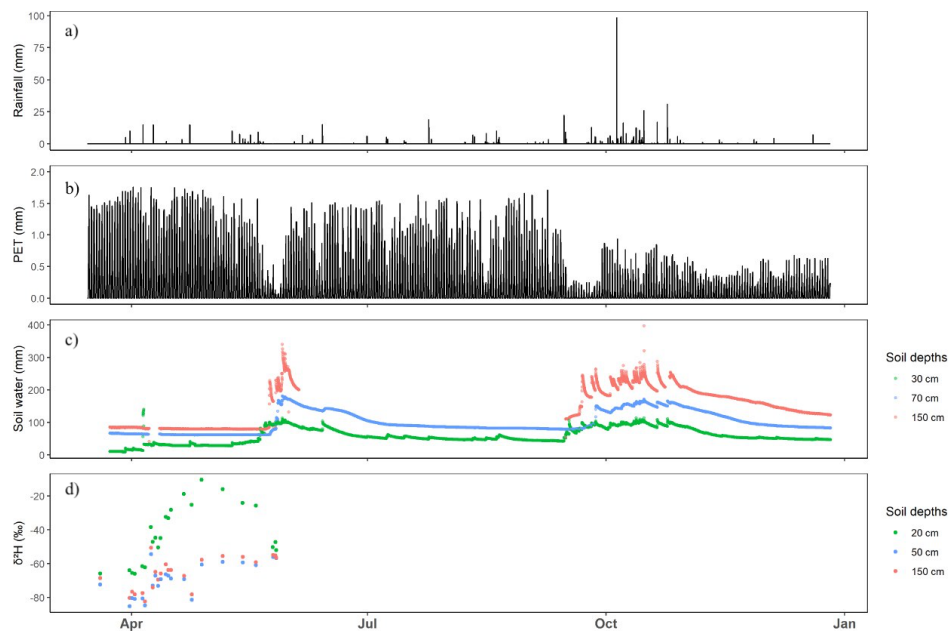
Figure 3. Time series of (a) precipitation, (b) potential evapotranspiration, soil water at different depths (c) corresponding to the upper, lower, and deep storage, and isotopic composition of soil water at 20 cm, 50 cm, and 150 cm (d).

Despite the low rainfall in the dry season, the water content in the soil presents values of up to 84 mm at a depth of 150 cm, as shown in Figure 3c. The maximum values of soil water content in October overlap with the maximum values of precipitation and lower values of potential evapotranspiration.

The time series of soil isotopes at a depth of 30 cm of the upper layer presents more significant variability, compared to the time series at a depth of 70 and 150 cm, following the isotopic behavior of rainfall (Figure 3d). In deeper soil layers, the variability is attenuated with more negative values, indicating little evaporation. The enriched isotopic signatures of the upper soil horizon indicate that an evaporative fractionation process occurs.

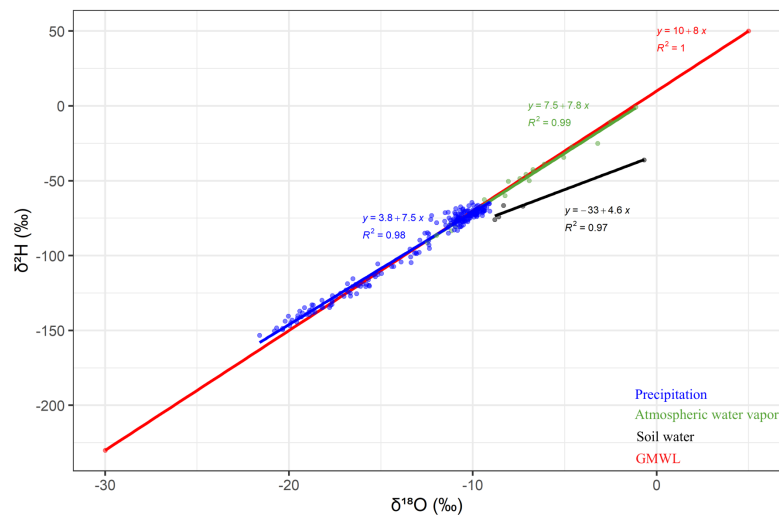**Figure 4.** Dual graph of isotopic composition of precipitation (blue), atmospheric water vapor (green), and soil water (black), accompanied by its Local Evaporative Line (LEL). The Global Meteoric Water Line (GMWL) is represented with the red line.

The precipitation isotopic values are close to the Global Meteoric Water Line, while the atmospheric water vapor values are more depleted due to the phase change (Figure 4). As a result, soil water composition exhibits a diversion in the slope, coherent with evaporative fractionation.

4.2. Hydrodynamic and Isotopic Simulations

Table 7 summarizes the results based on different objective functions for calibration. For the hydrodynamic module, the best metrics correspond to objective 1(a) (Table 5). While the calibration target 1(b) and 1(c) could not be reached because the maximum value of KGE4 is -0.1. Regarding the isotopic module, the best metric results correspond to 2(a), even though it does not meet the OF due to the KGE5 values of -0.29 and KGE7 of -0.13. Although 2(d) presents lower values of KGE5 and KGE7 than 2(a), it obtains values of KGE1 of 0.45 and KGE2 of 0.20. Notwithstanding the negative KGE values, KGE values greater than -0.41 imply that the model is better than the average of the observed data (Knoben et al. 2019).

Concerning the combination of both modules, 3(a) manages to better simulate the hydrodynamics in the soil reservoirs and, reasonably, the isotopic behavior in the second reservoir and atmospheric vapor. Conversely, 3(b) more successfully simulates the isotopic behavior in the second reservoir and atmospheric water vapor but only manages to replicate acceptably the dynamics in the first and third reservoirs.

Figure 5 displays the outcoming simulated soil water in the upper, lower, and deep reservoirs obtained from parameter sets of calibrations 3(a) and 3(b). Both calibrations capture the first reservoir's storage quite well (KGE1 of 0.45 Table 7); however, 3(b) underestimates the high peaks in June. As of July, 3(a) overestimates storage in the reservoir despite mimicking the dynamics. Concerning the simulation in the second reservoir, 3(b) fails to reproduce the behavior well in periods of maximum rainfall (October). Notwithstanding having KGE3 of 0.41 in 3(a), the third reservoir presented the worst fit between simulations and observed data, which may be caused by the missing period of observations from June to September.

Figure 6 presents the generated simulations of evaporation fluxes (in soil and interception), transpiration, and potential evapotranspiration (AET) of 3(a) and 3(b) calibrated models. 3(b) simulates lower evaporation flux values than 3(a), being more noticeable from October.

13

The opposite occurs with transpiration fluxes because it predicts higher fluxes throughout the period. Both OFs fail to replicate actual evapotranspiration because they overestimate the AET values, which is more evident for 3(b).

The resulting simulations of 3(a) and 3(b) of fluxes (Percolation, GW flow, and recharge) and actual evapotranspiration (AET) are shown in Figure 7. Generally, 3(b) shows lower values of fluxes than 3(a), more evidently in the period from April to October. 3(b) calibrated model is more restrictive with the vertical flux because as it deepens, the amount of flux decreases and results in values less than 0.3mm of recharge. These results are related to the difference in saturated hydraulic conductivity between the models ($kse3$ of 11 for 3(a) and $kse3$ of 6.5 for 3(b) Table 7).

Figure 8 shows the isotopic simulations of the models calibrated with 3(a) and 3(b). Both calibrated models lack to predict isotopic composition in the upper reservoir, despite having considered the fractionation process, with similar values of KGE5 (-0.35 and -0.36 Table 7). Overall, the hydrodynamic-focused calibrated model 3(a) reproduces more depleted isotopic signatures in the lower and deep reservoirs (note the scale difference on the *y-axis* in Figure 8) and exhibits limitations in simulating atmospheric water vapor compositions. On the other hand, the model focused on isotope 3(b) tests quite successfully the behavior and variability of the isotopic signals in the second reservoir and atmospheric water vapor.

The 3(a) calibrated model meets with the five objective functions. This model presents the best metrics in the hydrodynamic module and reasonably captures the isotopic dynamics. Given the prior, the vertical flows for each month were calculated based on this simulation (Table 8). The months of March, November, and December exhibit AET values greater than precipitation, obtaining AET/P ratios greater than 1. The most considerable flux occurs from the second to the third reservoir (Gwflow), with a total of 317 m from March to December 2019. This is partly because the lower reservoir presents the highest saturated hydraulic conductivity ($ks3$ Table 7). October presents the maximum recharge value of the period with 43.5 mm, overlapping with the maximum rainfall peak. From March to December 2019, there was a total recharge of 89 mm.

Table 7. Calibrated model parameter sets for each module with KGE values (n number of combined OF).

Calibration data	rE	alpha	Smax	Ic	ks1	ks2	ks3	GWmax	Lmax	g1	g2	g3	PF_Scale	INTp	stoSp	gwSp	lowSp	k	x	KGE1	KGE2	KGE3	KGE4	KGE5	KGE6	KGE7	KGE8
Hydrodynamic																											
1(a) (n=3)	-0.15	1.6	494	57.6	15.0	17.0	11.0	348	490	2.1	3.0	3.6	0.75	98	530	47	39	0.35	0.43	**0.45**	**0.48**	**0.41**	**-0.25**	**-0.35**	**0.07**	**-0.46**	**0**
1(b) (n=1)	-0.38	1	402	57.6	7.7	12.3	17.2	342	224	2.3	4.5	3.8	0.59	63	978	85	19	0.47	0.65	0.25	0.23	-0.25	-0.1	-0.33	0.32	-0.83	0.02
1(c) (n=4)	-0.38	1	402	57.6	7.7	12.3	17.2	342	224	2.3	4.5	3.8	0.59	63	978	85	19	0.47	0.65	0.25	0.23	-0.25	-0.1	-0.33	0.32	-0.83	0.02
Isotopic																											
2(a) (n=3)	-0.22	1.2	410	57.6	3.9	9.4	5	348	472	3.7	4.7	4.8	0.65	73	233	20	75	0.83	0.51	-0.2	0.34	-0.24	-0.19	-0.29	0.5	-0.13	0.02
2(b) (n=1)	-0.37	4.2	658	57.6	11.5	6.2	11.8	283	216	3.7	5	3.6	0.12	51.3	380	61	4.6	0.89	0.6	-1.05	-0.59	-1.27	-0.14	-0.26	0.05	-0.57	0.10
2(c) (n=4)	-0.22	1.2	410	57.6	3.9	9.4	5	348	472	3.7	4.7	4.8	0.65	73	233	20	75	0.83	0.51	-0.2	0.34	-0.24	-0.19	-0.29	0.5	-0.13	0.02
2(d) (n=2)	-0.39	2.2	468	57.6	11.7	9.5	6.5	359	484	2	4.7	3.8	0.79	87	407	10	88	0.8	0.39	**0.45**	**0.2**	**-0.05**	**-0.14**	**-0.36**	**0.61**	**-0.27**	**0.069**
Combined																											
3(a) (n=5)	-0.15	1.6	494	57.6	15.0	17.0	11.0	348	490	2.1	3.0	3.6	0.75	98	530	47	39	0.35	0.43	**0.45**	**0.48**	**0.41**	**-0.25**	**-0.35**	**0.07**	**-0.46**	**0**
3(b) (n=4)	-0.39	2.2	468	57.6	11.7	9.5	6.5	359	484	2	4.7	3.8	0.79	87	407	10	88	0.8	0.39	**0.45**	**0.2**	**-0.05**	**-0.14**	**-0.36**	**0.61**	**-0.27**	**0.069**

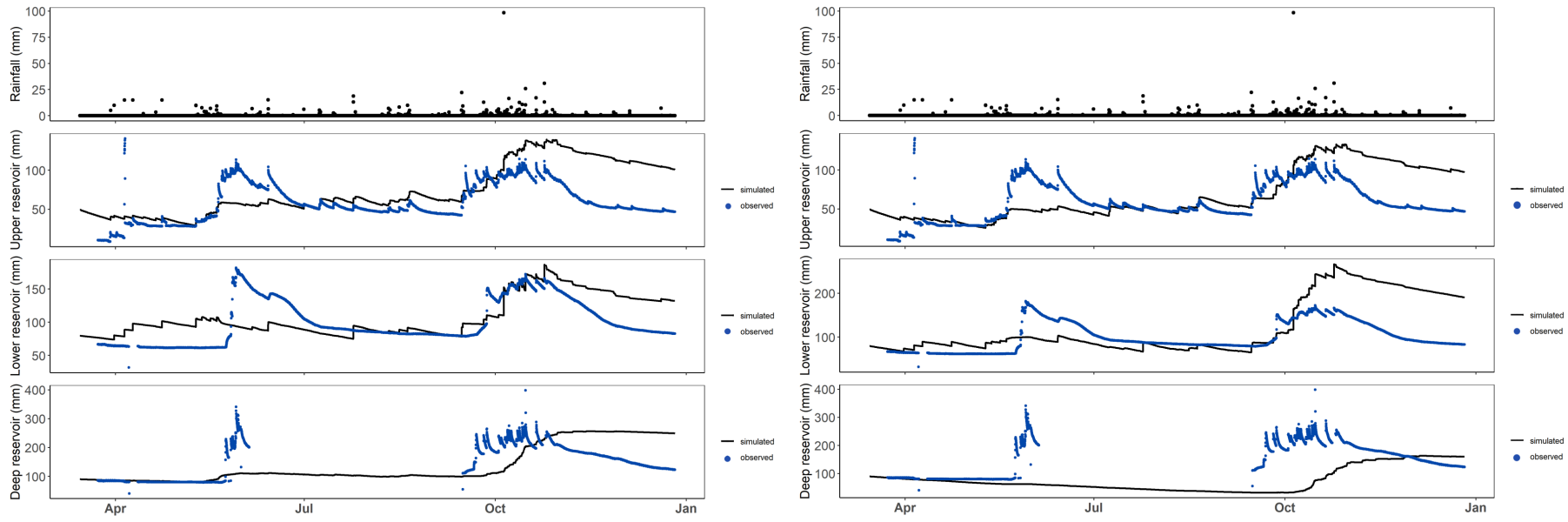Note that what is marked in **bold** presents the best combined results.

Figure 5. Outcoming simulated soil water in the upper, lower, and deep reservoirs in the studied plot at EEFH obtained from parameter sets of calibrations 3(a)-left and 3(b)-right. Precipitation is shown on top of the graph.
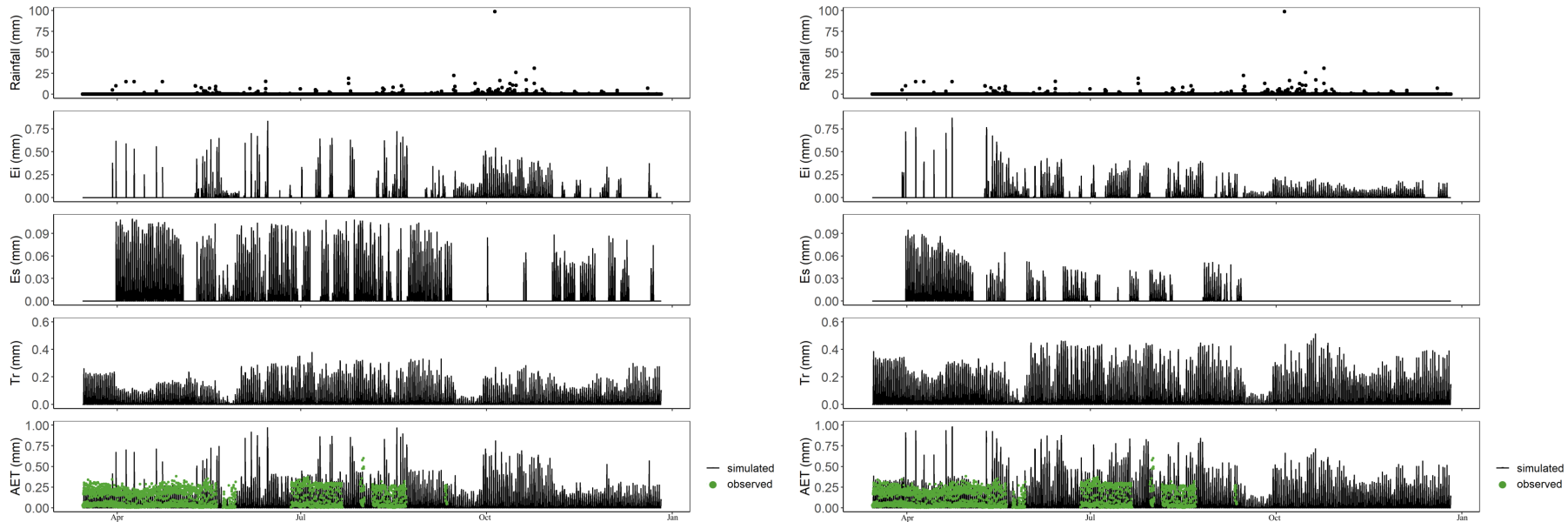
Figure 6. Simulations of 3(a)-left and 3(b)-right of evaporation fluxes (interception evaporation Ei and soil evaporation Es), transpiration (Tr), and actual evapotranspiration (AET) of the studied plot at EEFH. Precipitation is shown on top of the graph.

Figure 7. Simulations of 3(a)-left and 3(b)-right of fluxes (Percolation, GW flow, and Recharge) and actual evapotranspiration (AET) of the studied plot at EEFH. Precipitation is shown on top of the graph.

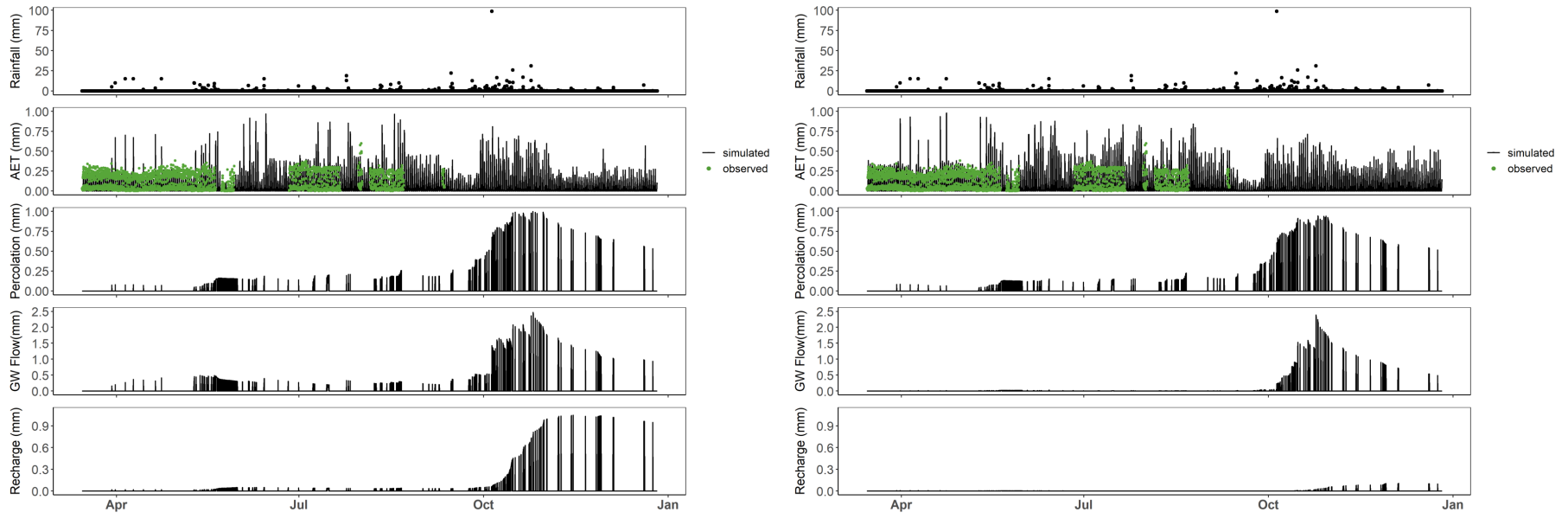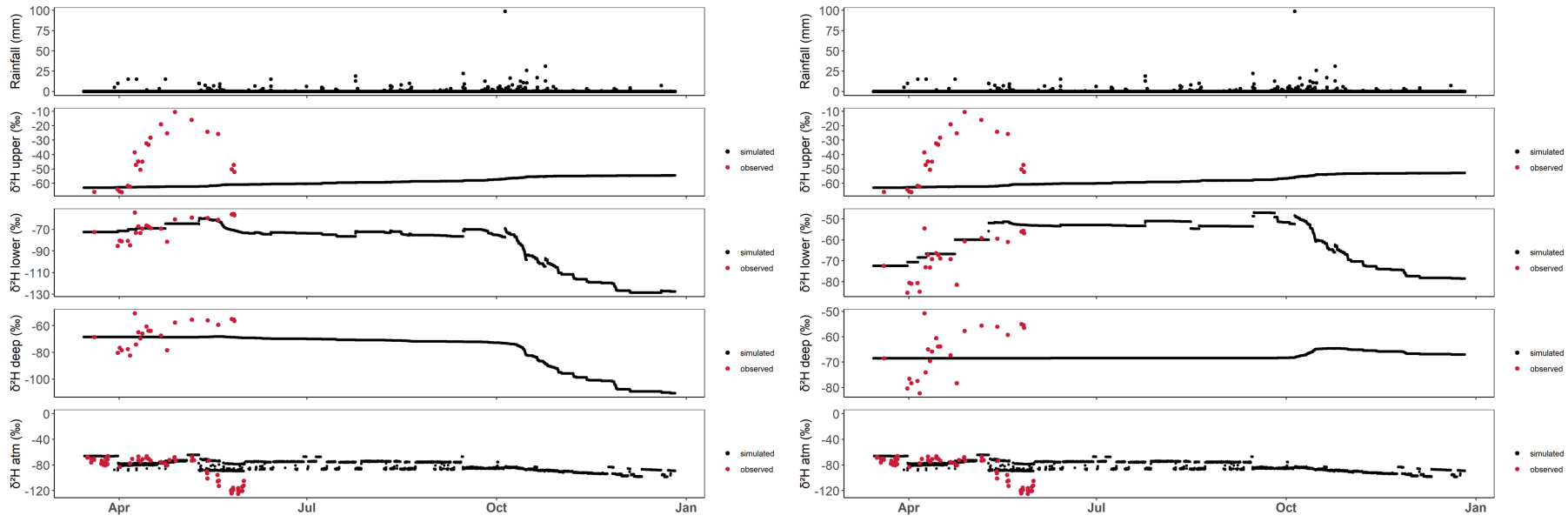**Figure 8.** Isotopic simulations of the models calibrated with 3(a)-left and 3(b)-right in the upper, lower, and deep storage, and atmospheric water vapor in the studied plot at EEFH. Precipitation is shown on top of the graph.

Table 8. Vertical fluxes and indexes based on 3(a) model simulations of the studied plot at EEFH from March to December 2019.

Months	P (mm)	Ei (mm)	Es (mm)	Tr (mm)	AET (mm)	Perc (mm)	GWFlow (mm)	Recharge (mm)	Tr/P	AET/P	Perc/P	GWFlow/P	Recharge/P
Mar	15	2.7	0.6	25.4	28.7	0.2	0.4	0.04	1.69	1.9	0.01	0.02	0.003
Apr	50.4	4.2	18.2	22.5	44.9	0.4	1.7	0.09	0.45	0.9	0.01	0.03	0.002
May	89.4	14.4	6.5	19.4	40.2	11.9	35.8	2.7	0.22	0.5	0.1	0.4	0.03
Jun	53.2	11.8	10.8	36.7	59.3	3.9	7.7	1.2	0.69	1.1	0.07	0.1	0.02
Jul	71.4	19.4	10.9	41.5	71.7	6.2	7.7	1.4	0.58	1.0	0.09	0.1	0.02
Aug	65	18.9	10.6	35.1	64.6	8.3	11.6	1.5	0.54	1.0	0.1	0.2	0.02
Sep	103.2	17.5	4.4	19.1	41.0	12.9	17.2	1.7	0.18	0.4	0.1	0.2	0.02
Oct	389.6	40.2	0.9	24.0	65.2	101.4	189.0	43.5	0.06	0.2	0.3	0.5	0.1
Nov	21	9.9	5.5	21.4	36.7	21.6	39.2	29.8	1.02	1.7	1.0	1.9	1.4
Dec	15	4.4	2.8	27.8	35.0	4.2	6.9	6.9	1.85	2.3	0.3	0.5	0.5
Total	*873.2*	*143.3*	*71.2*	*272.9*	*487.4*	*170.8*	*317.1*	*88.9*					

4. Discussion

The nineteen-parameter model presents the first approach to simulate vertical fluxes of water and tracers and storage dynamics in three soil horizons to estimate the aquifer recharge of a dry tropical forest in Costa Rica. The most balanced model was generated with a combined calibration of the hydrodynamic and isotopic feature (3(a) Table 7), which produced reasonable results for soil water storage, water fluxes, and isotopic behavior. Different calibration targets were considered because if calibration had considered only one criterion, this could mean model dismissal (Beven 2012).

We undertook that employing combined OFs for calibration would produce the most balanced model capable of adequately representing hydrodynamic and isotope processes. Representation of the most balanced model is a more achievable aim, considering that there are inevitable errors in the data and structures of hydrological models (Gupta et al. 2008).

The outcoming model is constituted of the vertical movement of water in the different soil horizons after a routine of interception and subsequent soil evaporation, interception evaporation, and soil transpiration. Infiltration reaches the upper reservoir, where a complete mixing of water and solutes occurs (mixing assumptions similar to Birkel et al. 2014 and Correa et al. 2020), draining nonlinearly to the next reservoir. The process is repeated in the lower and deep reservoirs until a non-linear recharge is reached. Mixing assumptions made in the models are known to cause uncertainties (Hrachowitz et al. 2013). Assuming complete mixing is not as accurate (Good et al. 2015). However, more parameters are required for partial mixing, which increases the uncertainties of the model (Correa et al. 2020). There is compensation for how many parameters may be needed to achieve a valid representation (Soulsby et al. 2008). Based on dominant processes, simple models with few parameters can generate realistic representations (Kirchner 2006). With this in mind, vertical variations of soil water isotopes at different depths were considered in the model, which improves the representation of infiltration (Beyer et al. 2020). We assume that incorporating soil isotope data will enable diverse aspects of the model to be evaluated (Seibert and McDonnell 2002).

Due to the potential non-conservative isotope behavior, fractionation by evaporation was considered in interception and soil. The model determines the isotopic content of the vapor from interception and the upper soil horizon. Usually, the incorporation in models of this process is unattended (Birkel et al. 2014), especially in the tropics water vapor is poorly characterized (Sánchez-Murillo et al. 2020). The above consideration resulted in satisfactory representations of the behavior and variability of the isotopic signals in atmospheric water vapor (Table 7 and Figure 8). Nonetheless, improvements are still required for the isotopic signals of the upper and deep reservoirs (Table 7 and Figure 8). Furthermore, given the results of KGE4 (Table 7), the improvement efforts in the model should be oriented to the simulation of transpiration, addressing that the quantification of this water flux is full of uncertainties (Kühnhammer et al. 2022).

Moreover, a first approximation of the estimation of aquifer recharge based on the simulations of the model was carried out. The growing risk of hydrometeorological extremes, which cause socioeconomic losses, can only be mitigated with measures based on solid knowledge of hydrological processes such as groundwater recharge (Mayer-Anhalt et al. 2022). The results in Table 8 show that a recharge of 89 mm was generated from March to December 2019. Presenting the maximum recharge value of 43.5 mm in October, consistent with the findings on the recharge of the Pacific of Costa Rica being favored in September and October (Sánchez-Murillo and Birkel 2016). Additionally, March, November, and December exhibit transpiration values (*Tr* Table 8) greater than precipitation, affecting the total AET and thus obtaining AET/P ratios greater than 1. The

latter could indicate that transpiration is a dominant water flux, similar to findings in a tropical rainforest in northern Costa Rica (Correa et al. 2020).

5. Conclusion

We developed the first approach of an hourly, lumped, conceptual, tracer-aided water balance model that simulates aquifer recharge in a dry tropical forest in Costa Rica. The nineteen-parameter model calculates vertical fluxes of water and tracers and storage dynamics in three soil horizons. The vertical water movement is determined after a routine of interception and subsequent soil evaporation, interception evaporation, and soil transpiration. The impact of specific data and objective functions (OF) for model calibration in flux and state simulations was evaluated. Different modules were addressed for calibration: hydrodynamic, isotope, and combined module. The most balanced model was generated with a combined calibration of the hydrodynamic and isotopic components, which produced reasonable results for soil water storage, water fluxes, and isotopic behavior (with KGE values between 0.45 and -0.46).

Besides, the model considers evaporative fractionation by estimating the isotopic content of the vapor losses from interception and the upper soil horizon, a commonly overlooked process. The incorporation of fractionation in the model resulted in satisfactory representations of the behavior and variability of the isotopic signals in atmospheric water vapor. Nevertheless, the isotopic composition in the upper and deep reservoirs is so far improperly depicted, which implies improvements in the conceptualization for better simulations.

Finally, a first effort was made to estimate the recharge based on the model with the best metrics. Simulations show that a recharge of 89 mm was generated from March to December 2019. Presenting the maximum recharge value of 43.5 mm in October.

6. References

Alfaro, E., Alvarado, A. and Chaverri, A. 2001. Cambios edaficos asociados a tres etapas sucesionales de bosque tropical seco en Guanacaste, Costa Rica!, Agron. Costarric., 25, 7–19 [online] Available from: https://www.semanticscholar.org/paper/CAMBIOS-EDAFICOS-ASOCIADOS-A-TRES-ETAPAS-DE-BOSQUE-Alfaro-Alvarado/753a56af9699ba2c3507a713795bf2f9fe693eb4.

Archana, S; Deodhar, Md; Ansari, A; Sharma, S; Nobel Jacob, U; Kumar, S; Singh, G. 2014. Isotope Techniques for Water Resources Management. Barc Newsletter (337):29-35.

Beven, K. 2006. A manifesto for the equifinality thesis. Journal of Hydrology 320: 18–36. DOI: https://doi.org/10.1016/j.jhydrol.2005.07.007.

Beven, K. 2012. Rainfall-runoff modelling. 2nd ed. Lancaster, UK, Wiley-Blackwell. 472 p. DOI: https://doi.org/10.1201/9780429423116-33.

Beyer, M; Kühnhammer, K; Dubbert, M. 2020. In situ measurements of soil and plant water isotopes: A review of approaches, practical considerations and a vision for the future. Hydrology and Earth System Sciences 24(9):4413-4440. DOI: https://doi.org/10.5194/hess-24-4413-2020.

Birkel, C; Soulsby, C; Tetzlaff, D. 2014. Water Resources Research. Water Resources Research RESEARCH 50:3481– 3501. DOI: https://doi.org/10.1002/2013WR014979.Reply.

Brauman, KA. 2015. Hydrologic ecosystem services: linking ecohydrologic processes to human well- being in water research and watershed management. (online). Wiley Interdisciplinary Reviews: Water 2(4):345-358. Consulted 1 jul. 2021. Available on http://doi.wiley.com/10.1002/wat2.1081

Correa, A; Birkel, C; Gutierrez, J; Dehaspe, J; Durán-Quesada, AM; Soulsby, C; Sánchez-Murillo, R. 2020. Modelling non-stationary water ages in a tropical rainforest: A preliminary spatially distributed assessment. Hydrological Processes 34(25):4776-4793. DOI: https://doi.org/10.1002/hyp.13925.

Echeverría Bonilla, J. 2011. Evaluación de la Vulnerabilidad Futura del Sistema Hídrico al Cambio Climático. San José, Costa Rica, Instituto Meteorológico Nacional. p. 88.

Farzamian, M; Monteiro Santos, FA; Khalil, MA. 2017. Constraining Unsaturated Hydraulic Parameters Using the Latin Hypercube Sampling Method and Coupled Hydrogeophysical Approach. Pure and Applied Geophysics 174(12):4471-4487. DOI: https://doi.org/10.1007/s00024-017-1656-1.

Gibson, JJ; Birks, SJ; Edwards, TWD. 2008. Global prediction of δA and $\delta 2H$- $\delta 18O$ evaporation slopes for lakes and soil water accounting for seasonality. Global Biogeochemical Cycles 22(2):1-12. DOI: https://doi.org/10.1029/2007GB002997.

Gibson, JJ; Birks, SJ; Yi, Y; Moncur, MC; McEachern, PM. 2016. Stable isotope mass balance of fifty lakes in central Alberta: Assessing the role of water balance parameters in determining trophic status and lake level. Journal of Hydrology: Regional Studies 6:13-25. DOI: https://doi.org/10.1016/j.ejrh.2016.01.034.

Gonfiantini, R; Wassenaar, LI; Araguas-Araguas, L; Aggarwal, PK. 2018. A unified Craig-Gordon isotope model of stable hydrogen and oxygen isotope fractionation during fresh or saltwater evaporation (online). Geochimica et Cosmochimica Acta 235:224-236. DOI: https://doi.org/10.1016/j.gca.2018.05.020.

Gonfiantini, R. 1986. Environmental isotopes in lake studies, in Hand- book of Environmental Isotope Geochemistry, edited by P. Fritz and J. C. Fontes, pp. 113–168, Elsevier, New York.

Good, SP; Noone, D; Bowen, G. 2015. Hydrologic connectivity constrains partitioning of global terrestrial water fluxes. Science 349(6244):175-177. DOI: https://doi.org/10.1126/science.aaa5931.

Gupta, H; Wagener, T; Liu, Y. 2008. Reconciling theory with observations: elements of a diagnostic approach to model evaluation (online). Hydrological Processes 22(November 2008):3802-3813. DOI: https://doi.org/10.1002/hyp.

Gupta, H. V.; Kling, H., Yilmaz, K. K.; & Martinez, G. F. 2009. Decomposition of the mean squared error and NSE performance criteria: Implications for improving hydrological modelling. Journal of hydrology 377(1-2): 80-91. DOI: doi:10.1016/j.jhydrol.2009.08.003.

GWP. 2016. Situación de los Recursos Hídricos en Centroamérica: Costa Rica. s.l., GWP Centroamérica. p. 40.

Horita, J; Wesolowski, DJ. 1994. Liquid-vapor fractionation of oxygen and hydrogen isotopes of water from the freezing to the critical temperature. Geochimica et Cosmochimica Acta 58(16):3425-3437. DOI: https://doi.org/10.1016/0016-7037(94)90096-5.

Hrachowitz, M; Savenije, H; Bogaard, TA; Tetzlaff, D; Soulsby, C. 2013. What can flux tracking teach us about water age distribution patterns and their temporal dynamics? Hydrology and Earth System Sciences 17(2):533-564. DOI: https://doi.org/10.5194/hess-17-533-2013.

IAEA (International Atomic Energy Agency). 2004. Isotope Hydrology and Integrated Water Resources Management. International Symposium held in Vienna, 19-23 May 2003 by IAEA and IAH in cooperation with the IAHS (May):19-23

IMTA (Instituto Mexicano de Tecnología del Agua). 2009. Laboratorio de Hidrología Isotópica. (online). Consulted jul. 2021. Available on: http://www.atl.org.mx/index.php?option=com_content&view=article&id=1371:laboratorio-de- hidrologia-isotopica&catid=133:aboratorio&Itemid=598

Instituto Meteorológico Nacional. 2020. Data from the meteorological station at the airport Daniel Oduber in Liberia, Guanacaste, Costa Rica, (online). Consulted 25 jul. 2021. Available on: https://www.imn.ac.cr/en/inicio

Iraheta, A. 2019. Partición isotópica de agua verde y azul en Costa Rica. s.l., CATIE. 74 p.

Kirchner, JW. 2006. Getting the right answers for the right reasons: Linking measurements, analyses, and models to advance the science of hydrology. Water Resources Research 42(3). DOI: https://doi.org/10.1029/2005WR004362.

Knoben, WJM; Freer, JE; Woods, RA. 2019. Technical note: Inherent benchmark or not? Comparing Nash-Sutcliffe and Kling-Gupta efficiency scores. Hydrology and Earth System Sciences 23(10):4323-4331. DOI: https://doi.org/10.5194/hess-23-4323-2019.

Kühnhammer, K; Dahlmann, A; Iraheta, A; Gerchow, M; Birkel, C; Marshall, JD; Beyer, M. 2022. Continuous in situ measurements of water stable isotopes in soils, tree trunk and root xylem: Field approval. Rapid Communications in Mass Spectrometry 36(5). DOI: https://doi.org/10.1002/rcm.9232.

Leiva, JA; Mata, R; Rocha, OJ; Gutiérrez Soto, M V. 2009. Cronología de la regeneración del bosque tropical seco en Santa Rosa, Guanacaste, Costa Rica. I. Características edáficas. Revista de Biologia Tropical 57(3):801-815. DOI: https://doi.org/10.15517/rbt.v57i3.5494.

Mayer-Anhalt, L; Birkel, C; Sánchez-Murillo, R; Schulz, S. 2022. Tracer-aided modelling reveals quick runoff generation and young streamflow ages in a tropical rainforest catchment. Hydrological Processes 36(2):2016-2017. DOI: https://doi.org/10.1002/hyp.14508.

Merlivat, L. 1978. Molecular diffusivities of H216O, HD16O, and H218O in gases. The Journal of Chemical Physics 69(6):2864-2871. DOI: https://doi.org/10.1063/1.436884.

Ortega, L; Gil, L. 2019. Isotope hydrology: An overview. s.l., s.e., vol.60. p. 4-5.

Powers, J. S., Becknell, J. M., Irving, J. and Pèrez-Aviles, D. 2009. Diversity and structure of regenerating tropical dry forests in Costa Rica: Geographic patterns and environmental drivers, For. Ecol. Manage., doi:10.1016/j.foreco.2008.10.036.

Sánchez-Murillo, R; Birkel, C. 2016. Groundwater recharge mechanisms inferred from isoscapes in a complex tropical mountainous region. Geophysical Research Letters 43(10):5060-5069

Sánchez-Murillo, R; Birkel, C. 2016. Groundwater recharge mechanisms inferred from isoscapes in a complex tropical mountainous region. Geophysical Research Letters 43(10):5060-5069. DOI: https://doi.org/10.1002/2016GL068888.

Sánchez-Murillo, R; Esquivel-Hernández, G; Birkel, C; Correa, A; Welsh, K; Durán-Quesada, AM; Sánchez-Gutiérrez, R; Poca, M. 2020. Tracing Water Sources and Fluxes in a Dynamic Tropical Environment: From Observations to Modeling. Frontiers in Earth Science 8(November):1-25. DOI: https://doi.org/10.3389/feart.2020.571477.

Sánchez-Murillo, R; Esquivel-Hernández, G; Welsh, K; Brooks, ES; Boll, J; Alfaro-Solís, R; Valdés- González, J. 2013. Spatial and Temporal Variation of Stable Isotopes in Precipitation across Costa Rica: An Analysis of Historic GNIP Records. Open Journal of Modern Hydrology 3(October):226- 240

Schlaepfer, DR; Ewers, BE; Shuman, BN; Williams, DG; Frank, JM; Massman, WJ; Lauenroth, WK. 2014. Terrestrial water fluxes dominated by transpiration: Comment. Ecosphere 5(5):1-9. DOI: https://doi.org/10.1890/ES13-00391.1.

Seibert, J; McDonnell, JJ. 2002. On the dialog between experimentalist and modeler in catchment hydrology: Use of soft data for multicriteria model calibration. Water Resources Research 38(11):23-1-23-14. DOI: https://doi.org/10.1029/2001wr000978.

SENARA. 2016. Plan de Aprovechamiento Sostenible de los Acuíferos Costeros del Cantón de Santa Cruz, Guanacaste. Guanacaste, Costa Rica, Servicio de Aguas Subterráneas, Riego y Avenamiento. p. 25.

SENARA. 2020. Manual de gestión participativa de acuíferos. Guanacaste, Costa Rica, Servicio de Aguas Subterráneas, Riego y Avenamiento. p. 23.

Soulsby, C; Neal, C; Laudon, H; Burns, DA; Merot, P; Bonell, M; Dunn, SM; Tetzlaff, D. 2008. Catchment data for process conceptualization: simply not enough? (en línea). Hydrological Processes 22(November 2008):2057-2061. DOI: https://doi.org/10.1002/hyp.

Sutanto, SJ; Wenninger, J; Coenders-Gerrits, AMJ; Uhlenbrook, S. 2012. Partitioning of evaporation into transpiration, soil evaporation and interception: A comparison between isotope measurements and a HYDRUS-1D model. Hydrology and Earth System Sciences 16(8):2605-2616. DOI: https://doi.org/10.5194/hess-16-2605-2012.

Waring, B. G., Pérez-Aviles, D., Murray, J. G. and Powers, J. S. 2019. Plant community responses to stand-level nutrient fertilization in a secondary tropical dry forest, Ecology, doi:10.1002/ecy.2691.

Werden, L. K., Alvarado J., P., Zarges, S., Calderón M., E., Schilling, E. M., Gutiérrez L., M. and Powers, J. S. 2018. Using soil amendments and plant functional traits to select native tropical dry forest species for the restoration of degraded Vertisols, J. Appl. Ecol., doi:10.1111/1365-2664.12998.